Investigating Earth's Formation History Through Copper and Sulfur Metal-Silicate Partitioning During Core-Mantle Differentiation

B. Mahan, J. Siebert, I. Blanchard, J. Badro, E. Kubik, P. Sossi, F. Moynier

Journal of Geophysical Research: Solid Earth

RESEARCH ARTICLE
10.1029/2018JB015991

Key Points:
- Modeling Earth's formation from chondritic material generates bulk silicate Earth Cu contents; however, this generates an overabundance of S
- Co-accretion of metal and silicate chondrules, akin to those in CH chondrites, can generate bulk silicate Earth abundances for Cu and S
- Cu results indicate that most chondritic materials require ~75% of Earth's accretion via incremental growth to reach minimum BSE Cu contents

Supporting Information:
- Supporting InformationS1

Correspondence to:
B. Mahan,
mahan@ipgp.fr

Citation:
Mahan, B., Siebert, J., Blanchard, I., Badro, J., Kubik, E., Sossi, P., & Moynier, F. (2018). Investigating Earth's formation history through copper and sulfur metal-silicate partitioning during core-mantle differentiation. *Journal of Geophysical Research: Solid Earth*, *123*, 8349–8363. https://doi.org/10.1029/2018JB015991

Received 20 APR 2018
Accepted 2 SEP 2018
Accepted article online 6 SEP 2018
Published online 8 OCT 2018

Investigating Earth's Formation History Through Copper and Sulfur Metal-Silicate Partitioning During Core-Mantle Differentiation

B. Mahan[1], J. Siebert[1,2], I. Blanchard[1], J. Badro[1,3], E. Kubik[1], P. Sossi[1], and F. Moynier[1,2]

[1]Institut de Physique du Globe de Paris, Université Paris Diderot, Sorbonne Paris Cité, Paris, France, [2]Institut Universitaire de France, Paris, France, [3]Earth and Planetary Science Laboratory, Ecole Polytechnique Fédérale de Lausanne, Lausanne, Switzerland

Abstract Identifying extant materials that act as compositional proxies for Earth is key to understanding its accretion. Copper and sulfur are both moderately volatile elements; however, they display different geochemical behavior (e.g., phase affinities). Thus, individually and together, these elements provide constraints on the source material and conditions of Earth's accretion, as well as on the timing and evolution of volatile delivery to Earth. Here we present laser-heated diamond anvil cell experiments at pressures up to 81 GPa and temperatures up to 4,100 K aimed at characterizing Cu metal-silicate partitioning at conditions relevant to core-mantle differentiation in Earth. Partitioning results have been combined with literature results for S in Earth formation modeling to constrain accretion scenarios that can arrive at present-day mantle Cu and S contents. These modeling results indicate that the distribution of Cu and S in Earth may be the result of accretion largely from material(s) with Cu contents at or above chondritic values and S contents that are strongly depleted, such as that in bulk CH chondrites, and that the majority of Earth's mass (~3/4) accreted incrementally via pebble and/or planetesimal accretion.

Plain Language Summary Experiments wherein molten metal and silicate (rock-building) phases unmix themselves due to their physical properties, that is, metal-silicate partitioning, can be conducted at the high temperatures and pressures (HP-HT) that characterized Earth's differentiation into a core and mantle. The redistribution of elements between the metal and silicate phases—their partitioning—during this process can be measured and mathematically described, then placed into numerical models to better understand Earth's formation history. Here we have mathematically characterized the HP-HT partitioning of copper, combined this with results for sulfur from literature, and input these characterizations into numerical models that track their distribution between Earth's core and mantle as it grows to its present mass. Copper and sulfur were chosen because they display different sensitivities to the physical mechanisms that govern planetary formation, and we can leverage this to better understand Earth's formation and differentiation history. Our results indicate that ~75% of Earth's precursor materials grew incrementally from relatively small bits of material—on average ~0.1% of Earth's mass or less—that is most compositionally similar to meteorite classes that are made up of iron-rich metal and silicate solids (chondrules) that are depleted in easily vaporized (volatile) elements, especially sulfur.

1. Introduction

Earth's formation is considered to be the result of the agglomeration and accretion of large planetesimals, wherein impacts provide the kinetic energy necessary to melt the majority of the proto-Earth, leading to the development of a deep magma ocean (perhaps multiple times; Chambers, 2004; Halliday & Wood, 2009; Li & Agee, 1996; Tonks & Melosh, 1993; Wetherill, 1989). Such melting engendered wholesale gravitational separation of immiscible metal and silicate liquids at high pressure and temperature, that is, core/mantle differentiation, thereby significantly altering the chemical and isotopic distribution of elements in Earth (Georg et al., 2007; Hin et al., 2013; McDonough & Sun, 1995; Shahar et al., 2011; Wood et al., 2006). However, this synopsis is largely schematic, as Earth's source material and its homogeneity (or not), the conditions and timing of its differentiation and volatile delivery, and the proportion of material that accreted as giant impacts are all still widely debated (e.g., Albarède, 2009; Badro et al., 2007, 2014; Bottke et al., 2010; Brenan & Mcdonough, 2009; Corgne et al., 2008; Dreibus & Palme, 1996; Halliday, 2013; Hin et al., 2013; Laurenz et al., 2016; Li & Agee, 1996; Mahan et al., 2017; Morard et al., 2013; Piet et al., 2017; Rubie et al.,

2015, 2016; Savage et al., 2015; Schönbächler et al., 2010; Seagle et al., 2006; Siebert et al., 2011; Suer et al., 2017; Wade & Wood, 2005; Wade & Wood, 2016; Wade et al., 2012; Wohlers & Wood, 2015; Zhang et al., 2016). Experimental metal-silicate partitioning at high pressures and temperatures that encompass those of terrestrial core formation (up to 75 GPa, >3,500 K; e.g., Badro et al., 2015; Fischer et al., 2015; Siebert et al., 2012, 2013) are key to further understanding planetary differentiation, as they do not require extrapolation of data from lower *P-T* conditions.

Copper is a moderately volatile, siderophile, and chalcophile element with a 50% nebular condensation temperature (T_{50}) of ~1,037 K (Lodders, 2003). It is depleted in the bulk silicate Earth (BSE) compared to the Sun and chondritic meteorites (Lodders & Fegley Jr, 1998; Palme & Jones, 2003; Palme & O'Neill, 2014), and this depletion is twofold in origin. It is due to volatility-related processes, as attested to by the depletion of lithophile elements with similar T_{50} (e.g., K, 1,006 K or Na, 958 K) in the BSE (Palme & O'Neill, 2014), and to being further depleted due to its partial sequestration into Earth's core (e.g., Siebert & Shahar, 2015, and references therein). Sulfur is also a moderately volatile element but is more volatile than Cu with T_{50} of around 700 K (Lodders, 2003). Furthermore, it is *the* chalcophile element of reference in an Earth science context (though *chalcos* actually refers to Cu; Goldschmidt, 1922). As such, although the siderophilities of Cu and S both decrease with increasing temperature (e.g., Righter et al., 2010; Suer et al., 2017), the relative magnitude of this change is different, and as such their disparate behaviors can be leveraged to resolve details of Earth's formation history. Despite the differing volatilities of these two elements, their co-investigation is strongly supported given that isotopic evidence for a multitude of elements—Ga, Cu, K, Rb, Zn, S, Se, and Cd (from least to most volatile)—suggests that Earth's depletion in moderately volatile elements cannot be attributed to significant volatile loss during accretion and is therefore largely inherited from its source material(s) (e.g., Kato & Moynier, 2017; Luck et al., 2005; Pringle & Moynier, 2017; Pringle et al., 2017; Sossi et al., 2018; Vollstaedt et al., 2016; Wang & Jacobsen, 2016; Wombacher et al., 2008). Moreover, the abundances of Cu and S in most Solar System materials display quite a strong correlation, as the ratio of Cu to S (Cu/S) is relatively constant across chondritic materials in spite of their difference in volatility under nebular conditions, with Cu/S in fact showing less variation than Zn/S (e.g., Lodders & Fegley Jr, 1998).

In summary, these observations strongly suggest that the abundances of Cu and S in the BSE together with those in its core, that is, bulk Earth (BE), should add up to those in its source materials. With this in mind, the synthesis of partitioning data for these elements in numerical modeling of Earth's accretion and core formation provides a means to generate the abundances of these elements in the BSE (and the core), thereby testing plausible source materials and accretion scenarios that could have largely set the budget of these elements in Earth's main layers (e.g., Dreibus & Palme, 1996; Mahan et al., 2017). Although numerous studies have investigated the metal-silicate partitioning of Cu (Corgne et al., 2008; Holzheid & Lodders, 2001; Righter et al., 2010; Schmitt et al., 1989; Vogel, 2015; Wood et al., 2014), none of them have parameterized its metal-silicate partitioning at conditions directly applicable to core-mantle differentiation in Earth and have relied on extrapolations from lower *P-T* conditions.

Here we report Cu metal-silicate partitioning results at high pressures and temperatures (49–81 GPa and 3,500–4,100 K, respectively) from laser-heated diamond anvil cell experiments. These experiments are part of an ongoing collaboration investigating metal-silicate partitioning of a suite of elements, with Cu being the focus of the current study, and selected results for other elements being published elsewhere (e.g., K, U in Blanchard et al., 2017; Mn in Siebert et al., 2018; Zn in Mahan, Siebert, et al., 2018). Partitioning results have been combined with those in the literature (Corgne et al., 2008; Righter et al., 2010; Vogel, 2015; Wood et al., 2014) to produce a robust thermodynamic parameterization of Cu metal-silicate partitioning across a very broad range of pressure and temperature (1–81 GPa and 1,773–4,100 K) that fully encompasses the conditions of core formation in Earth. We have then input these results, along with those for S from literature, into continuous Earth formation models, wherein numerous controls were evaluated, namely, source materials, the onset of large impacts, and the timing and evolution of volatile delivery. In an effort to alleviate the well-established discrepancies between the volatile budgets of Earth and bulk chondritic material, which may not be attributable to appreciable volatile loss, we have evaluated compositional proxies (not absolute matches) for Earth that include volatile depleted, chondrule-like materials, which circumvent any necessity for volatile loss. We have also evaluated metal-rich carbonaceous chondrite-like material (e.g., CH chondrites) as proxies for the accretion of both metal and silicate chondrules, thus alleviating Fe deficiencies generally

Table 1
P, T, ΔIW, and logK_e Values

Starting material	Experiment	P (GPa)	T (K)	ΔIW	logK_e[a]	σ/2SE[b]
Diamond anvil cell experiments						
Fe + PYR[c]	*PYR K Fe 40*	54	4,000	−1.07	0.55	0.17
	PYR K Fe 60	71	4,100	−0.84	0.44	0.11
M238[d] + PYR	*PYR K FeS 40*	49	3,700	−0.89	0.54	0.07
Fe + S238[e]	*BAS K Fe 40*	49	3,500	−0.91	0.49	0.15
	BAS K Fe 60	70	3,700	−0.60	0.28	0.07
	BAS K Fe 70	81	4,000	−0.62	0.29	0.07
M238 + S238[e]	*BAS K 52*	62	3,600	−0.59	0.46	0.07
	BAS K 62	72	3,700	−0.68	0.48	0.13
Large volume press experiments						
FeS + MORB	*E205*	2	1,673	−1.27	2.45	0.19
	E206	2	1,673	−1.31	2.39	0.16
	E208	2	1,873	−1.22	2.25	0.14
Fe-FeS + MORB	*E238*	2	1,673	−1.26	2.52	1.49[f]
Fe + MORB	*E291*[g]	2	2,200	−2.69	1.89	0.27
	E294[g]	2	2,025	−2.96	1.88	0.33
Fe + KLB1	*E295*[g]	2	2,200	−3.35	1.83	0.27
	E296[g]	2	2,300	−3.35	1.77	0.17

[a]logK_e values for all S-bearing experiments have been corrected for the influence of S on Cu metal-silicate partitioning after Wood et al. (2014). [b]In line with convention, 1 sigma error reported for DAC experiments, and 2SE error reported for P-C experiments. [c]PYR (abbrev. pyrolite) made from high purity oxides and carbonates. [d]M238 designates the metallic fraction of piston cylinder experiment 238. [e]S238 designates the basaltic (silicate) fraction of piston cylinder experiment 238. [f]Large propagated error for E238 due to a low accelerating voltage for this measurement (not included in Figure 2). [g]Piston-cylinder experiments ran in BN capsules (as opposed to MgO); capsule material had no effect on partitioning.

associated with chondrule accretion. These models have been used to hone in on plausible scenarios that can arrive at present-day estimated abundances of Cu and S in the BSE while maintaining low levels of S in Earth's core.

2. Methodology

2.1. Starting Materials

For piston-cylinder experiments, two silicates—one basaltic and one peridotitic (KLB1 composition)—were used for the silicate phases (70 wt. % of bulk), in conjunction with either a nominally pure metallic Fe or (Fe and S) alloy (30 wt. % of bulk), in either MgO or BN capsules. All bulk starting materials (metal + silicate) were doped with 1–2 wt. % powdered Cu metal to ensure measurable quantities of Cu, namely, in the postexperiment silicate fraction. Each starting material was dry-mixed in an agate mortar and pestle for 15–20 min to ensure a compositionally homogeneous starting mixture.

For DAC experiments, two compositionally distinct silicate glasses were produced as magma ocean analogues, one from a mid-ocean ridge basalt (MORB), and the other a synthetic pyrolite. The synthetic pyrolite was produced by mixing high-purity oxide and carbonate powders doped with approximately 5 wt. % K and 1 wt. % each of Cu, Zn, Pb, and U that were then ground under ethanol in an agate mortar, dried, and cold-pressed to produce chips. These chips were then melted in an aerodynamic laser levitation furnace at the Institut de Physique du Globe de Paris (IPGP) under a pure O_2 atmosphere (to minimize loss of volatiles such as Cu), equilibrated and quenched to produce glass beads approximately 1–2 mm in diameter (after Auzende et al., 2011). The MORB glass was produced in a metal-silicate partitioning experiment ("E238") in a 150 ton, end-loaded piston-cylinder apparatus at IPGP. The starting material for this experiment contained 70 wt. % MORB and 30 wt. % metallics (50/50 mix of Fe metal and stoichiometric FeS from powders). This mixture was then doped with approximately 5 wt. % K and 1 wt. % each of Cu, Zn, Pb, and U. The high S content of E238 was chosen as it considerably reduces the melting temperature of the metallic phase (Buono & Walker, 2011) and produces metal and silicate phases with appreciable S, such that both were viable S-bearing starting materials for subsequent DAC experiments. Representative pieces of glasses (basalt and pyrolite) and the S-rich metal from E238 were then mounted and polished and checked for textural and compositional homogeneity via scanning electron microscope (SEM) imaging and electron microprobe (EPMA) analysis. Compositional data for starting materials have been reported in Table S1 in the supporting information. The basaltic and pyrolytic glasses were then polished on both sides down to a wafer of constant thickness (~20 μm) from which small disks were laser machined to 70- to 120-μm diameters (depending on subsequent DAC configurations) using a picosecond laser machining instrument (IPGP). The S-rich metal from piston-cylinder experiment E238 was ground to a fine powder for loading into DAC charges. For S-poor and nominally S-free experiments, spherical Fe powder (Alfa Aesar, 5 μm, 99.9 + % metal basis) was used for the metallic phase.

2.2. Piston-Cylinder Experiments

All experiments were conducted in the piston-cylinder apparatus at IPGP at a pressure of 2 GPa in ½" cell assemblies, over the full range of allowable temperatures, that is, those book-ended by sample melting and furnace limitations (1,673–2,300 K). Experiments were heated with a cylindrical graphite furnace and temperatures measured with a top-loaded Type D thermocouple, with either a talc-pyrex or barium carbonate ($BaCO_3$) pressure medium, depending on temperature conditions, with the latter used temperatures above 1,600 °C for its superior thermo-insulation properties. Both MgO or BN capsules were used in order to assess any influence of these materials on Cu partitioning. Run durations were chosen to ensure elemental equilibrium while also mitigating capsule interaction with the experimental charge. Compositions (wt. %) for

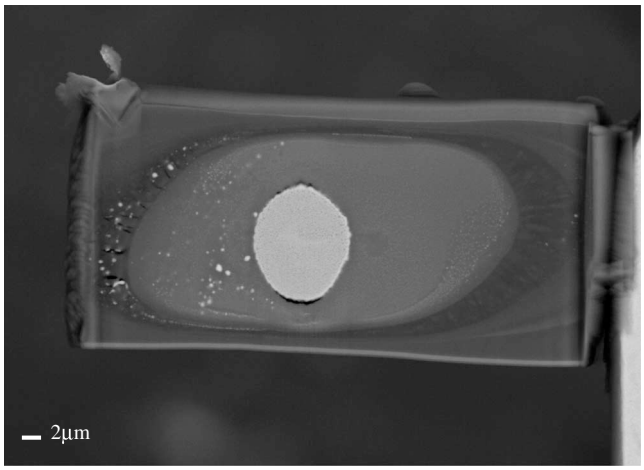

Figure 1. Backscatter electron image of a typical DAC experiment ("PYR K FeS 40" shown). A large main metallic spherule (white/gray) displaying sulfide quench texture, surrounded by an a-crystalline silicate matrix (light gray), with small, stranded metallic globules (bright spots) dispersed within the silicate fraction. An envelope of unheated, and therefore unmelted and unreacted, silicate (dark gray) envelopes the entire experimental charge. The lighter color of the molten silicate is due to increased FeO content relative to the starting material (i.e., unmelted silicate), in agreement with previous observations (Blanchard et al., 2017; Fischer et al., 2015; Siebert et al., 2012).

all experiments can be found in Table S1, and experimental conditions are reported in Table 1. All experiments were quenched under pressure by cutting power to the resistive heater.

2.3. DAC Experiments and Sample Recovery

Prior to experimentation in the diamond anvil cell, Raman shift calibration of the diamond couplets were conducted such that pressure could be determined directly from this parameter (Akahama & Kawamura, 2004), thereby avoiding any possible chemical contamination associated with use of ruby fluorescence. Rhenium plates of ~1 cm^2 (h = 250 μm) were pre-indented to achieve a *Re* gasket thickness of 40–50 μm, which were laser machined to produce a central hole with a diameter slightly larger than the sample disks, then placed back on the bottom diamond culet (d = 200–300 μm, depending on target pressure). Sample loading was achieved by first centering a silicate disk inside the gasket hole, on top of which either the S-rich metallic powder or spherical Fe metal powder was placed and centered, and finally, a second silicate disk was placed atop this, completing the sample assembly. This configuration allows for efficient differentiation of the metal and silicate phases during experimentation and furthermore employs the silicate disks as both sample material and pressure medium due to their thermally and chemically insulating properties, which localize the hot zone of the experiments and mitigate carbon contamination from the diamonds (Badro et al., 2016; Siebert et al., 2013).

Experiments were first brought to pressure, then heated on both sides using a split-beam 200 W infrared fiber laser. Temperatures were continuously measured by fitting spectroradiometric data taken from both sides of the DAC with a Planck function (Benedetti & Loubeyre, 2004). Target temperatures were achieved within 30–60 s of experimental outset, accompanied by complete melting in the focus region of the laser, which is evidenced by a plateau in temperature as a function of laser power (e.g., Lord et al., 2010). Experiments were held in a super-liquidus state for 20–30 s (postplateau) to ensure complete chemical differentiation and equilibration (Siebert et al., 2012), then quenched by cutting power to the laser system. Final pressure were corrected for thermal expansion with a $\Delta P_{thermal}$ of ~2.5×10^{-3} GPa/K (Fiquet et al., 2010; Siebert et al., 2012). Conditions for all experiments are reported in Table 1. Uncertainties for experimental pressure and temperature scale with magnitude and are approximately 4% and 7%, respectively (e.g., Badro et al., 2016).

Recovery of samples was carried out with a focused ion beam (FIB) instrument coupled to a field emission SEM (FE-SEM) at IPGP. Prior to sample excavation, an ~1–μm-thick strip of Pt was applied to the top of the section for protection from ion bombardment. Thin sections of 20 × 30 × 3 μm were then excavated from the center of the hot spot along the compressional axis, characterized by a small metallic spherule (d ≈ 10 μm) surrounded by quenched glassy matrix (Figure 1). Upon completion of excavation, an in situ micromanipulator is used to recover samples from the *Re* gasket and emplace them on a TEM grid using a Pt weld. Finally, samples are polished with the FIB at low current for subsequent compositional analysis via electron microprobe (EPMA).

2.4. Elemental Analysis (EPMA)

Elemental composition for both piston-cylinder and DAC experiments, along with the pyrolite starting material and the S-rich metal, were analyzed using a CAMECA SX Five EPMA at the CAMPARIS facility in Paris (Université Pierre et Marie Curie and IPGP, Paris). Operating conditions were 15-kV accelerating voltage with a 40-nA beam current, with counting rates of 10–20 s on background and peak for major elements and 20–40 s on background and peak for minor elements. Metal and silicate phases from DAC experiments were first analyzed using EDX spectroscopy on the FE-SEM (15 keV and 5-nA beam current) for ground-truth of complete metal-silicate differentiation and qualitative analysis, followed by quantitative analysis via EPMA. Data attained by EDX and EPMA were indistinguishable within error, indicating a lack of analytical artifacts (e.g., TEM grid contamination). Operating conditions for EPMA analyses were 20-keV accelerating voltage

with a 20-nA beam current (1-μm spot size) with counting times of 10–20 s on background and peak for all elements. Minerals and pure oxides were used as standards for all elements.

For piston-cylinder experiments, multiple representative pieces of 30-μm diameter (or greater) of metal and silicate phases from all experimental runs were mounted and polished in hardened resin, then carbon coated prior to analysis. Averages from multiple (>10) 20- to 30-μm^2 beam rasters were used to determine compositions for both metal and silicate phases, and as such, errors for piston-cylinder data are conventionally reported as 2SE. For all DAC experiment phases, averages from multiple (≥3) beam spots were used to determine bulk compositions, with error for DAC data reported as one standard deviation (σ), in accordance with convention. Metallic phases often display heterogeneities along the interface with the surrounding silicate, resulting from nucleation and mass diffusion processes upon quenching (O'Neill et al., 1998), and therefore, all measurements were confined to the inner ⅔ of the metallic spherules. Many experiments contained submicron metallic globules trapped in the silicate melt phase that failed to coalesce with the main metallic spherule, either as a result of adhesive/cohesive forces or from viscous entrapment in the silicate melt. Due to their small size, reliable analysis of these stranded metallic globules was not possible and these were avoided during analysis of the silicate phase. Compositional data for all experiments have been reported in Table S1.

2.5. Thermodynamic Formalization

The thermodynamics of Cu metal-silicate partitioning can be described by the redox reaction,

$$CuO_{1/2}^{silicate} + \frac{1}{2}Fe^{metal} = \frac{1}{2}FeO^{silicate} + Cu^{metal} \quad (1)$$

where Cu is considered monovalent (1+) in the silicate melt (Schmitt et al., 1989; Vogel, 2015) and therefore the equilibrium constant, K, of this reaction can be written as

$$\log K = \log \frac{\left(X_{FeO}^{silicate}\right)^{1/2} * \left(X_{Cu}^{metal}\right)}{\left(X_{CuO_{1/2}}{}^{silicate}\right) * \left(X_{Fe}^{metal}\right)^{1/2}} + \log \frac{\left(\gamma_{Cu}^{metal}\right)}{\left(\gamma_{Fe}^{metal}\right)^{1/2}} + \log \frac{\left(\gamma_{FeO}^{silicate}\right)^{1/2}}{\left(\gamma_{CuO_{1/2}}{}^{silicate}\right)} \quad (2)$$

where the first term on the right side of this equation is the exchange coefficient of the reaction as calculated from experiments, K_{Cu}^{D}. Iron and Cu oxide activity coefficient ratios do not vary considerably (Righter et al., 2010; Siebert et al., 2011; Wade & Wood, 2005), and the influence of silicate composition and structure is negligible, rendering a simplified expression for the equilibrium constant,

$$\log K_e = \log K_{Cu}^{D} + \log \frac{\left(\gamma_{Cu}^{metal}\right)}{\left(\gamma_{Fe}^{metal}\right)^{1/2}} \quad (3)$$

where $\log K_e$ is the *effective* (calculated) logarithm of the equilibrium constant and activity coefficients for the metals are calculated via the interaction parameter approach described by Ma (2001). This approach allows the use of tabulated interaction parameters (ε) in order to calculate activity coefficients (?; The Japan Society for the Promotion of Science and The Nineteenth Committee on Steelmaking, 1988), wherein a positive ε value indicates decreased siderophility of an element, and vice versa. Of particular note in terms of planetary differentiation, the presence of S in the metal phase is known to influence the partitioning of trace elements (e.g., Chabot & Agee, 2003) and thus where applicable corrections have been made for the influence of S on Cu metal-silicate partitioning following Wood et al. (2014; $\varepsilon_{Cu}^{S} = -2.57$). An interaction parameter for Si, $\varepsilon_{Cu}^{Si} = 0.73$, was determined by Vogel (2015); however, such a small value renders the influence of Si essentially negligible, such that the data of Vogel (2015) can be faithfully reproduced without it (e.g., Figure 30a of reference), and therefore, for simplicity, this has not been included in our data treatment. A negative ε value for O is reported in the Steelmaking Data Sourcebook, whereas a positive, but comparable magnitude ε value for C has been reported (e.g., Corgne et al., 2008; 3.98 and −3.57, respectively), which would lead to an increase in the siderophility of Cu with increasing O content, and vice versa for C. However, these values have not been well constrained within the context of HP-HT metal-silicate differentiation, and therefore, only nominally C-free experiments have been included in our thermodynamic parameterization, and the influence of O in the metal phase has not been included.

Once $\log K_e$ values have been calculated, it is then possible to isolate and describe the various thermodynamic controls on Cu metal-silicate partitioning by expressing its partitioning behavior through the relation

$$\log K_e = a + \frac{b}{T} + \frac{c*P}{T} \quad (4)$$

where a, b, and c are regression constants determined via least squares multivariable regression; T is temperature in K; and P is pressure in GPa. This method follows previous studies (Blanchard et al., 2015; Corgne et al., 2008; Mahan et al., 2017; Righter et al., 1997; Siebert et al., 2011, 2013; Wade & Wood, 2005), and further details can be found therein. Using this expression for the logarithm of the equilibrium constant, the regression constant a is the intercept (proportional to the entropy change of reaction), and constants b and c describe the sensitivity of the elements partitioning to temperature (enthalpy change of reaction) and pressure (volume change of reaction), respectively. Finally, oxygen fugacity (fO_2) relative to the iron wüstite (IW) buffer is be calculated via

$$\Delta \mathrm{IW} = 2 \log \frac{\left(\boldsymbol{X}_{\mathrm{FeO}}^{\mathrm{silicate}}\right)}{\left(\boldsymbol{X}_{\mathrm{Fe}}^{\mathrm{metal}}\right)} \quad (5)$$

where ideal mixing behavior for Fe in both silicate and metallic melts has been assumed, and therefore, ΔIW values reported in this manner are minima (see Siebert et al., 2011).

3. Results

3.1. Phase Morphology, Texture, and Composition

All DAC experiments were conducted at conditions exceeding the liquidus of both metal and silicate phases, resulting in a main metallic or sulfide spherule of ~10 μm in diameter enveloped in quenched glass enriched in FeO relative to the starting material (Table S1 and Figure 1), with both phases containing quench features consistent with other studies (Chidester et al., 2017; Fischer et al., 2015; Siebert et al., 2012, 2013; Suer et al., 2017). Many experiments contained secondary submicron globules in the silicate phase, interpreted as metal droplets which failed to coalesce with the main metallic spherule (Figure 1). Backscatter electron (BSE) imaging indicate the absence of exsolved "nano-nuggets" of metal in the silicate phase, confirming no cross-contamination of phases in the EPMA analyses.

The composition of the metal/sulfide and silicate phases from piston-cylinder experiments, including that used to generate DAC starting materials (E238), and the composition of all DAC experiments are reported in Table S1. Electron microprobe data for elements of interest in concomitant works have been excluded from the metallic phase; however, compositional totals (wt. %) include all EPMA data. Errors for all EPMA measurements of DAC experiments are reported as 1SD (σ). Errors for piston cylinder experiments are reported as 2SE to account for integration of local heterogeneities, as previously discussed (Chabot et al., 2009; Mahan et al., 2017; Mahan, Siebert, et al., 2018; Siebert et al., 2011).

3.2. Copper Exchange Coefficients

Exchange coefficients (Table 1) are inversely correlated with temperature; that is, the affinity of Cu for the metallic/sulfide phase decreases with increasing temperature, in accord with previous observations (Corgne et al., 2008; Righter et al., 2010; Vogel, 2015). Exchange coefficients are also inversely correlated with pressure (Table 1 and Figure 2), an effect unconstrained in previous works at lower pressures.

4. Discussion

4.1. Thermodynamic Controls on Cu Metal-Silicate Partitioning

Diamond anvil cell data from this study, as well as data from piston-cylinder experiments (where available; $\log K_e$, T, and P; see Table 1), have been combined with literature data (Corgne et al., 2008; Righter et al., 2010; Vogel, 2015; Wood et al., 2014; N° = 59) to characterize Cu metal- and sulfide-silicate partitioning across a broad range of temperatures (1,673–4,100 K). In order to determine any possible effect of pressure, this data compilation spans a much broader range of pressures (1–81 GPa) than previous works, confined to below 21 GPa and below 2,900 K (e.g., Vogel, 2015). All data, along with model P-T paths of $\log K_e$, can be found in

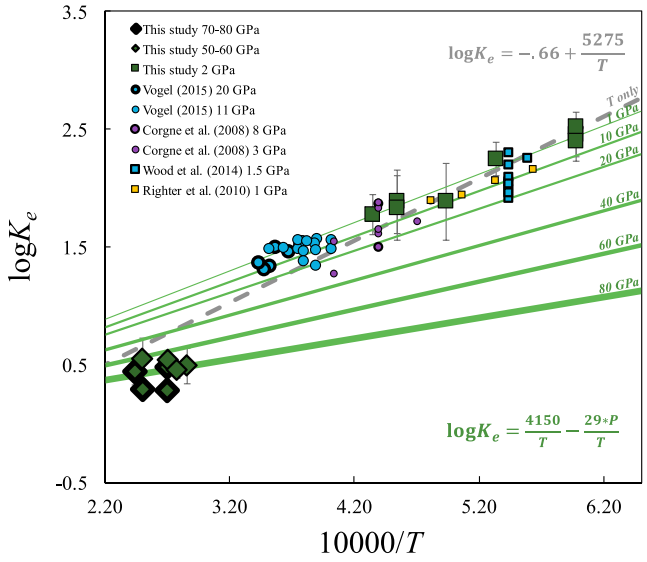

Figure 2. Exchange coefficients, logK_e, plotted as a function of reciprocal temperature (10,000/T). Diamond anvil cell experiments from the current study are indicated by green diamonds, and piston-cylinder experiments are indicated by green squares, with a thicker border denoting higher experimental pressure. Data from literature (Corgne et al., 2008; Righter et al., 2010; Vogel, 2015; Wood et al., 2014) are designated as in the legend with average pressure; thicker borders indicate higher pressures within each study. All data display an increase in logK_e as a function of reciprocal temperature; that is, as temperature increases, the siderophility of Cu decreases. Experiments display a modest decrease in logK_e with increasing pressure, a trend constrained with the addition of DAC data in the current work. Sulfur-bearing experiments have been corrected for the effect of S on metal-silicate partition coefficients (Wood et al., 2014). Model *P-T* paths for logK_e have been constructed using resolved coefficients from equation (4) ($a = 0.0 \pm 0.1$, $b = 4150 \pm 303$, and $c = -29 \pm 6$; see sections 2.5 and 4.2 for details). Pressure is qualitatively represented by thickness of the solid green lines, wherein increasing thickness indicates increasing pressure. The dotted gray line represents a regression model for all data considering only temperature ($a = -0.66 \pm 0.11$, $b = 5275 \pm 254$), indicating that a temperature dependence alone does not sufficiently describe the metal-silicate partitioning of Cu across the entire *P-T* range.

Figure 2. The data regression yielded constants of $a = 0.0 \pm 0.1$, $b = 4{,}150 \pm 303$ (K), and $c = -29 \pm 6$ (K/GPa). These results represent the first thermodynamic characterization of Cu metal-silicate partitioning including DAC data at high pressure and temperature and are the first to resolve a statistically significant effect of pressure on Cu metal-silicate partitioning, which significantly dampens the siderophility of Cu at pressures relevant to core formation in Earth. These regression results strongly indicate that the partitioning of Cu between metal and silicate can sufficiently be described as a function of temperature and pressure alone, without need of invoking sensitivity to silicate composition and/or possible structural changes at high pressure (Morard et al., 2007; Sanloup et al., 2013; Wang et al., 2016), and by approximating Si and O ε values as null.

4.2. Numerical Modeling of Earth's Accretion and Core Formation

4.2.1. General Framework

The regression constants calculated above can be used to evaluate various Earth formation models (using equation (4)) based on their ability to generate BSE abundances for Cu and S and do so utilizing parameterizations for these elements that encompass plausible *P-T* conditions for Earth's formation and thus do not rely on extrapolation. The models herein follow a paradigmatic accretion pathway, wherein the size of accreting objects increases with time, finalized by a large impact of 9.5% the mass of Earth (M_E) that may have formed the Moon, and a late veneer of 0.5% M_E of CI-like material. Copper and S concentrations in the primitive mantle (~BSE) of 20 ± 10 and 200 ± 80 ppm, respectively, were taken from Palme and O'Neill (2014) as pass/fail criteria for model results. As the siderophility of Cu largely inhibits its presence in the BSE, the following models focus on achieving a minimum Cu content of 10 ppm. Numerous lines of evidence indicate that the S content of Earth's core can be no more than ~2 wt. % (e.g., Badro et al., 2014, 2015; Dreibus & Palme, 1996), including the partitioning behavior of S at high pressure and temperature (Suer et al., 2017), which largely prohibits values above this, and as such all model results herein yield S contents in the Earth's core at or below 2 wt. %. The influence of S on Cu partitioning, both in the growing Earth and in accreting impactors, has been included in the modeling, as its presence increases the siderophility of Cu (e.g., Wood et al., 2014). Oxygen fugacity (fO_2) was fixed at ΔIW-2.3 in all models to provide a median outcome and to mitigate model proliferation. Temperatures were bound by the peridotite liquidus (averaged from Fiquet et al., 2010 and Andrault et al., 2011), and the pressure of magma ocean equilibration was set at 40% of that of the core-mantle boundary for each accretionary step (e.g., Siebert et al., 2012). As previously noted, all models inherently generate S contents in Earth's core of 2 wt. % or less due to the inclusion of S partitioning data (Suer et al., 2017), and such values are consistent across numerous disciplines (e.g., Badro et al., 2014; Dreibus & Palme, 1996; Zhang et al., 2016).

In order to provide a more comprehensive view of planetary formation, the effects of partial equilibration have been considered in our modeling via the formulation of Deguen et al. (2014). In this context, mixing occurs via turbulent entrainment of impact material with proto-Earth's mantle, and the efficiency of equilibration is determined by both the size of the impactor (relative to magma ocean depth) and the siderophility of the element(s) considered. The fraction of accreting metallic core material that equilibrates with the surrounding silicate mantle, denoted as k, varies with impactor size, wherein incremental growth (impactors ~0.1% M_E) has a $k = 1$ (i.e., 100% of metal equilibrates), and larger impactors (2% M_E or more) have a $k = 0.5$ (50% of metal equilibrates). This treatment of the k parameter is in line with that determined using W anomalies (30–80%, Nimmo et al., 2010; Rudge et al., 2010), however is lower than that suggested elsewhere (Fischer et al., 2017; Rubie et al., 2016) for matching highly siderophile element abundances in the mantle, and therefore, it should be noted that a higher fraction of equilibrating impactor metal serves to

increase the BSE abundances of Cu and S, and thus, our BSE model estimates may be lower bounds in this respect. The fraction of Earth's mantle that equilibrates with impactors increases with the size of proto-Earth due to the increasing depth of the magma ocean (i.e., the volume of mantle encountered) and generally produces a mass of equilibrating mantle that is on par with the mass of the impactor core itself. Further details can be found in Deguen et al. (2014), and its application to Earth formation modeling herein follows that described in Suer et al. (2017). A comprehensive discussion of the effects of parameter tuning (e.g., metal/silicate equilibration) is outside the scope of the current work; however, detailed analyses these variables can be found in Deguen et al. (2014), Rubie et al. (2015, 2016), and Fischer et al. (2017).

Wherever possible, present-day BSE and source material abundance estimates for Cu and S with the smallest possible associated errors have been utilized (e.g., Barrat et al., 2012; McDonough, 2003; Palme & O'Neill, 2014) to ensure the most robust results possible. However, errors for estimates are not always reported (e.g., Lodders & Fegley Jr, 1998), and the high number of degrees of freedom in planetary formation modeling quickly swells propagated errors far beyond utility. Moreover, the overarching aim of this work is to constrain plausible accretion scenarios, not to redefine or further constrain BSE and/or BE volatile element abundances. Therefore, model results are to be interpreted as qualitative observations used to discern between viable accretion histories.

The following models have focused on chondrule-rich accretion scenarios, which is by and large an iteration of pebble accretion, or the accretion of planetary materials from centimeter- to meter-sized objects. Such accretion mechanisms are of specific interest as they may have played an important role in terrestrial planet formation (e.g., Bollard et al., 2017; Cuzzi et al., 2008; Jacobsen & Walsh, 2015; Johansen et al., 2015; Levison et al., 2015), since chondrule-rich accretion can potentially explain volatile and moderately volatile element abundances in the BSE and BE (e.g., Amsellem et al., 2017; Hewins & Herzberg, 1996; Mahan, Siebert, et al., 2018; Righter et al., 2006), especially in the absence of appreciable volatile loss from Earth and other terrestrial bodies during accretion (e.g., Canup et al., 2015; Stewart et al., 2016). Moreover, chondrules likely provide a reliable record of the conditional and compositional evolution of the solar system during the planet-forming epoch (Libourel & Portail, 2018; Mahan, Moynier, et al., 2018). In the following models, both the size and volatile contents of Earth's accreting materials increase with time, culminating in a relatively volatile-rich, large impactor corresponding to 9.5% M_E toward the end of accretion. The accretionary process finishes with a late sprinkling of CI-like material of ~0.5% M_E (i.e., a "late veneer"), in line with conventional estimates (e.g., Brenan & Mcdonough, 2009). The overarching objective of the modeling being not to define *actual* source materials for Earth, but instead to constrain extant materials that can act as model building blocks.

The first models explore the viability of general chondrule accretion, where normative Cu and S abundances for chondrules have been used (100-ppm Cu and 6,400-ppm S), and the onset of large impacts (2% M_E or more) is varied to constrain pathways that can match primitive mantle Cu and S contents. These average Cu and S source material values are valid as there is a general agreement between elemental abundance and element-to-element ratios among chondrules in most chondritic materials, for example, the abundances (and ratios) of elements such as Cu and S in the chondrules of carbonaceous chondrites (e.g., Amsellem et al., 2017; Hezel et al., 2018). The variation in the onset of large impacts encompasses a generalized range of stochastic accretion pathways wherein Earth accretes from larger and larger impacts through time. Based on BSE Cu and S contents generated in these preliminary models, accretion from chondrules that are both enriched in Cu and depleted in S is explored, wherein CH chondrite chondrules have been used as an extant proxy material. Given that chondrules are generally deficient in Fe relative to Earth, these models are then followed by an accretion scenario for Cu which inherently considers the coaccretion of Fe-rich metal, which also function as chondrules/pebbles, alleviating this Fe-deficiency and simultaneously satisfying cosmochemical and astrophysical observations which suggest that much of the Fe in the early inner solar system was metallic (e.g., Pignatale et al., 2016, 2017; Rubie et al., 2015, 2016). As a compositional proxy for accretionary material characterized by volatile-poor chondrules and Fe-rich metal in this scenario, we have used bulk CH chondrite Cu contents. This is appropriate as CH chondrites are essentially pristine cosmic conglomerates of mostly Mg-rich chondrules (~70 vol. %) and FeNi metal (20–30 vol. %), with only minor amounts of matrix (~5 vol. %) and CAIs (0.1 vol. %; Ivanova & Petaev, 2015; Righter et al., 2006; Weisberg et al., 2006). Furthermore, they are exceptionally depleted in S both in the bulk and in their chondrules (Lodders & Fegley Jr, 1998; Bischoff et al., 1993, respectively). Given the likely suppressed siderophile behavior of S at HP-HT during Earth's

formation (Suer et al., 2017), this marked S depletion in Earth's initial source material in order to generate present-day S contents in the BSE (e.g., Mahan, Siebert, et al., 2018). With all this in mind, bulk CH chondrites may provide a viable model precursor material—but probably not actual precursor material—for Earth and other terrestrial planets.

There are currently no direct data for the Cu content of CH chondrules; therefore, Cu concentrations have been estimated by back-calculating from bulk CH chondrite Cu contents (120 ppm) to account for the diluting effects of FeNi metal, which comprises ~43 wt. % of the bulk and is thought to have been initially devoid of Cu (e.g., Campbell & Humayun, 2004). This calculation generates Cu chondrule concentrations for CH chondrules of 210 ppm. It should be noted that this estimate assumes a null effect of the matrix and/or other components, which may not be the case, as it is possible that minor, Cu-enriched components such as "hydrated lithic clasts" may significantly influence the overall budgets of these elements and thus the calculated chondrule Cu contents (e.g., Campbell & Humayun, 2004). This is an acceptable unknown, as the overall aim is simply to test a source material with enhanced Cu contents. Sulfur contents have been measured in CH chondrules and are generally well below ~700 ppm (Bischoff et al., 1993); here a normative value of 500 ppm has been assumed.

4.2.2. Constraining Earth's Source Material From BSE Cu and S During Accretion

A series of models were run investigating the evolution of BSE Cu and S contents as a function of accretion to assess the influence of source material volatile contents and partial equilibration on final BSE values. Broadly speaking, the bulk Cu contents of chondrules (and chondrites) define a relatively narrow range of Cu contents of around 100 ppm ± 50 ppm (e.g., Hezel et al., 2018, and references therein). For S, a chondrule concentration of 0.64 wt. % has been used as this describes median chondrule S contents (e.g., CO chondrules; Grossman & Wasson, 1983) while also representing S estimates for the BE itself (e.g., McDonough, 2003). From Figures 3a and 3b and Table 2 it is evident that the onset of large impacts (2% Earth's mass or more) must begin after over 85% of Earth's mass has accreted incrementally (i.e., from pebbles and/or planetesimals) in order to bring Cu levels in the BSE just into the acceptable range (~10 ppm). However, this is partially contingent on later heterogeneous arrival of more volatile-rich material (125-ppm Cu) in the last ~12% of accretion (9.5% as a giant impact), a pathway modeled for consistency with recent constraints for the Moon-forming giant impact (Piet et al., 2017; Wade & Wood, 2016). Exploring a similar path for S, modeled after Suer et al. (2017), wherein the onset of large impacts begins after 80% of accretion, but with no volatile enhancement in the last ~12% of accretion, that is, homogeneous accretion (as opposed to that modeled for Cu), quickly generates S contents in the BSE well above the accepted range defined (solid line, Figure 3b and Table 2). If the onset of large impacts in such a scenario begins much earlier, after 20% of Earth's mass has been accreted, BSE S contents can be generated (dotted line, Figure 3b and Table 2), but this is contingent on Earth having an effective embryo to incremental growth ratio (*E*/*I* hereafter) of ~4 or higher, and having no heterogeneous accretion of more volatile-rich material and/or a late veneer. Furthermore, as can be deduced from Figure 3a, such a scenario would be accompanied by a depletion in BSE Cu contents. These observations indicate that accretion from such material is largely at odds with current planetary formation paradigms (e.g., Rubie et al., 2015, 2016) and BSE composition (e.g., McDonough, 2003; Palme & O'Neill, 2014) and necessitates the exploration of potential building blocks that are relatively enriched in Cu and depleted in S.

Chondrules that fit this description are found in CH chondrites, estimated herein to have chondrule Cu contents of 210 ppm, and for which the measured chondrule S contents are ~500 ppm (Bischoff et al., 1993). Accretion from CH chondrite chondrule-like material, wherein the onset of large impacts begins after 20% of Earth's accretion (*E*/*I* ~4), with later addition of CI-like material during the last ~12% of accretion, generates BSE Cu contents just below the acceptable range with or without a late veneer (~8 ppm), and BSE S contents that are within the acceptable range without a late veneer (150 ppm), and just over it (300 ppm) with a late veneer (Figures 3c and 3d). Broadly speaking, these results suggest that accretion from such material may provide more viable pathways towards generating BSE Cu and S abundances, especially in regards to S.

For Cu, these results indicate the necessity for a higher fraction of incremental growth, as even complete incremental growth (fully equilibrating) would not achieve the present-day reported 20 ppm (see Figure 3a). This may also suggest that present-day estimates are too high, or that Earth accreted as-of-yet unidentified material with an augmented Cu content. For S, these results imply that in the absence of a

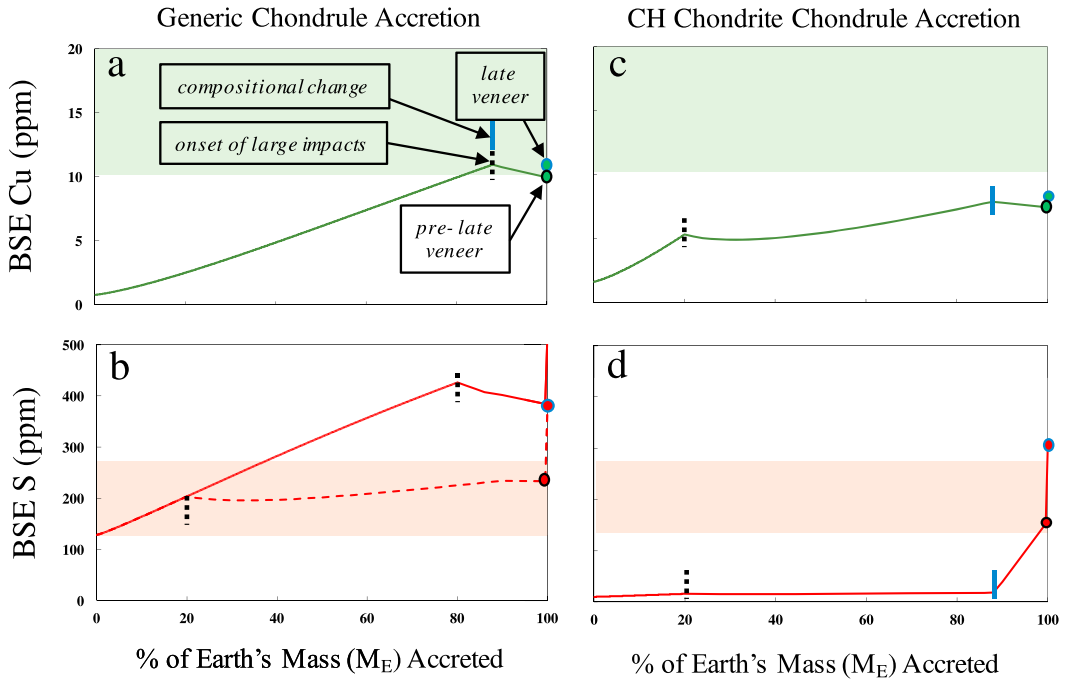

Figure 3. Evolution of BSE Cu (top row) and S (bottom row) contents as a function of Earth's accreted mass (%) for (first column) generic chondrule accretion and (second column) CH chondrite chondrule accretion. (a) BSE Cu evolution for incremental generic chondrule accretion (100-ppm Cu), followed by large impact accretion of CI-like material (125-ppm Cu) after 88% M_E has accreted. (b) BSE S evolution for incremental accretion of chondrule-/BE-like material (6,400-ppm S), where onset of large impacts occurs either at 20% M_E or 80% M_E. (c) BSE Cu evolution for incremental accretion of CH chondrite chondrules (210-ppm Cu) up to 20% M_E, followed by large impacts of the same composition until 88% M_E, where large impact accretion from CI-like material (125-ppm Cu) begins. (d) BSE S evolution along same accretion pathway as in (c), with 3,500-ppm S in CH chondrite chondrules and 54,100 ppm in the CI-like material. The green and red shaded regions represent acceptable BSE Cu and S contents (respectively) as determined by estimates of Palme and O'Neill (2014). As annotated in (a), the vertical black dashed lines indicate the onset of large impacts (2% of Earth's mass or more) and the vertical blue lines indicate a composition change to volatile-enriched, CI-like material; the black encircled points at 99.5% accretion represent BSE Cu (green) and S (red) contents prior to the addition of a late veneer, and the blue encircled point (100% accretion) represent BSE Cu (green) and S (red) contents after the addition of a CI-like late veneer of 0.5% Earth's mass. All source material compositions, as well as pre- and post-late veneer final BSE values for Cu and S for all models are reported in Table 2.

secondary mechanism that removed it from the BSE (and/or BE), the average S content of Earth's source materials was likely close to ~0.7 wt. % or less (approximated by mass balance of the two source materials), a value similar to that suggested for the BE (0.64 wt. %). Furthermore, from Figures 3b and 3d it is clear that generating present-day BSE S contents, especially while accommodating a late veneer, requires that this be heterogeneously distributed between an initial, S-poor material, followed by more S-rich material later in accretion, that is, through heterogeneous accretion. Accretion largely from a

Table 2
Summary of Modeling Results

Model	Source material (s)[a]	Source Cu (ppm)	Source S (ppm)	Large impacts	BSE Cu (ppm)[b]	BSE S (ppm)	Core Cu (ppm)	Core S (wt. %)
3a	Generic Chondrules/CI	100/125	6,400	12%	*10 [11]*		*300*	
3b	Generic Chondrule (BE)		6,400	20%		*380 [530]*		*1.9*
				80%		*230 [380]*		*1.9*
3c	CH Chondrules	210/125	500/54,100	80%	*7.5 [8.4]*		*600*	
3d	CH Chondrules/CI		500/54,100	80%		*150 [300]*		*2.0*
4	Bulk CH (chondritic) /CI	120/125	3,500/54,100	25%	*9.5 [10]*		*350*	

[a]Primary source material/secondary source material. [b]All values in italics are model results; values in [] indicate postlate veneer BSE contents.

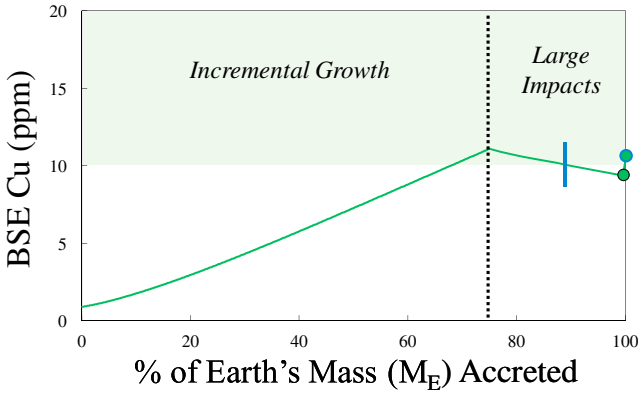

Figure 4. Evolution of BSE Cu contents from a chondritic source material (here bulk CH chondrites, 120-ppm Cu) as a function of Earth's accreted mass. In order to reach a minimum BSE Cu content of 10 ppm, approximately 75% of Earth's mass must accrete incrementally, here in the form of pebbles and/or planetesimals, with the final 25% of Earth accreting form large impacts which equilibrate with Earth's mantle to a lesser degree owing to their increased size. Such a scenario yields an embryo to incremental growth ratio *E/I* of approximately 0.3.

preferentially S-poor material is not at all contingent on Earth accreting mainly from large impactors, illustrated by the virtual lack of an inflection point in BSE S evolution at the onset of large impacts in Figure 3d, thus opening up possibilities for further incremental growth to reach minimum BSE Cu contents of ~10 ppm. Accretion largely from S-poor material also circumvents the need for late sulfur sequestration via exsolution, that is, through a so-called "Hadean Matte" (e.g., Laurenz et al., 2016; Rubie et al., 2016), as the BSE essentially never becomes S-saturated. It remains unclear whether this can be fully reconciled with the highly siderophile element suite (e.g., O'Neill, 1991; Rubie et al., 2016), as currently no data exists at relevant *P-T* conditions for these elements or for sulfide saturation. What is clear, however, is that such an event would essentially strip the BSE of its already minimal Cu contents, rendering any appreciable sulfide segregation at odds with the current work.

Despite the relative success of the CH chondrite chondrule model in generating acceptable BSE S contents, this scenario falls just shy of generating BSE Cu contents, does not account for the inherent Fe-depletion associated with chondrule accretion, and does not provide any constraints on the *E/I* ratio that characterized Earth's accretion. In order to obviate these issues, it is therefore requisite to constrain the level of incremental growth required to generate minimum present-day Cu contents, as well as to consider the co-accretion of both metal and silicate.

4.2.3. Constraining the Ratio of Embryos to Incremental Growth, *E/I*

Modeling accretion from bulk CH-like material is analogous to the co-accretion of both metal and silicate chondrules, yet maintains a broadly chondritic Cu content (120 ppm). It can thus provide first order constraints on the embryo to incremental growth ratio (*E/I*) leading to a minimum Cu BSE abundance (10 ppm). Simultaneously, such a model maintains consistency with BSE S contents and the BE Fe budget, thus providing first-order constraints on the minimum degree to which incremental growth could have contributed to Earth's accretion. As illustrated in Figure 4, these results suggest that incremental growth up to ~75% of Earth's mass through pebble and/or planetesimal accretion, or an E/I ration of ~0.3 (with the remainder accreting via larger impacts), can generate minimum BSE Cu contents. Such a proportion of incremental growth is in agreement with current constraints on chondrule accretion pathways for terrestrial planet formation, wherein chondrule contribution itself can reach half or more of the total, and along with planetesimal contributions can potentially account for the majority of planetary accretion (e.g., Johansen et al., 2015; Levison et al., 2015). Furthermore, this scenario is consistent with BSE S contents, as it is clear from Figure 3d that with a S-poor initial source material, the influence of large impacts is negligible, thereby rendering BSE S evolution from such material largely insensitive to *E/I*, and thus dominantly controlled by source material composition alone.

5. Conclusions

In this study, we have conducted a set of Cu metal-silicate partitioning experiments at HP-HT conditions (up to 80 GPa and 4,100 K) in both diamond anvil cells and a piston-cylinder apparatus, extending the pressure-temperature range well beyond that of previous works. These results represent the first parameterization of Cu metal-silicate partitioning from experiments that encompasses conditions directly comparable to Earth's core formation. The thermodynamic characterization presented herein indicates a small but measurable effect of pressure on Cu partitioning that was previously unresolved. Thermodynamic characterizations of Cu (this work) and S (literature results) metal-silicate partitioning were incorporated into a number of Earth formation models to assess potential source materials and viable accretion pathways. Cumulatively, these models suggest that Earth could have grown via the co-accretion of metal and silicate chondrules depleted in volatile elements, especially S, such that the majority (more than 3/4) of Earth's mass accreted in the form of pebbles and planetesimals, yielding an embryo to incremental growth ratio, *E/I*, of ~0.3 or less. Accretion along such a pathway satisfies numerous boundary conditions for Earth's formation, in that it

(1) raises BSE Cu contents to a minimum value, (2) keeps the BSE S budget sufficiently low, (3) accounts for the Fe budget of the BE, and does so while (4) allowing for heterogeneous later accretion of more volatile-rich material and (5) a late veneer.

Acknowledgments
We very kindly thank editor Michael Walter and our reviewers Paul Savage and Steve Elardo for their invaluable feedback, which has greatly improved the overall manuscript. We are indebted to Stephan Borensztajn for carrying out the FIB/SEM work. We also thank Nicolas Wehr for his expertise in the petrology lab, as well as Michel Fialin and Nicolas Rividi at the CAMPARIS facility for their expertise with the SX Five microprobe. We acknowledge the financial support of the UnivEarthS Labex program at Sorbonne Paris Cité (ANR-10-LABX-0023 and ANR-11-IDEX-0005-02). FIB and SEM instruments are supported by IPGP multidisciplinary program PARI and by Paris-IdF region SESAME grant 12015908. B.M. thanks the financial support of the IDEX SPC through a PhD fellowship. J.S. thanks the financial support of the French National Research Agency (ANR Project VolTerre, grant ANR-14-CE33-0017-01). J.B. acknowledges funding from the European Research Council under the European Community's Seventh Framework Programme (FP7/2007-2013)/ERC grant agreement 207467 (DECore). F.M. acknowledges funding from the European Research Council under the H2020 framework program/ERC grant agreement 637503 (Pristine), and the ANR through a *chaire d'excellence* Sorbonne Paris Cité. All original data used in calculating Cu metal-silicate equilibrium constants can be found in the supporting information for this paper, and modeling equations can be found in Suer et al. (2017).

References

Akahama, Y., & Kawamura, H. (2004). High-pressure Raman spectroscopy of diamond anvils to 250 GPa: Method for pressure determination in the multimegabar pressure range. *Journal of Applied Physics*, *96*(7), 3748–3751. https://doi.org/10.1063/1.1778482

Albarède, F. (2009). Volatile accretion history of the terrestrial planets and dynamic implications. *Nature*, *461*(7268), 1227–1233. https://doi.org/10.1038/nature08477

Amsellem, E., Moynier, F., Pringle, E. A., Bouvier, A., Chen, H., & Day, J. M. D. (2017). Testing the chondrule-rich accretion model for planetary embryos using calcium isotopes. *Earth and Planetary Science Letters*, *469*, 75–83. https://doi.org/10.1016/j.epsl.2017.04.022

Andrault, D., Bolfan-Casanova, N., Nigro, G. L., Bouhifd, M. A., Garbarino, G., & Mezouar, M. (2011). Solidus and liquidus profiles of chondritic mantle: Implications for melting of the Earth across its history. *Earth and Planetary Science Letters*, *304*(1), 251–259.

Auzende, A. L., Gillot, J., Coquet, A., Hennet, L., Ona-Nguema, G., Bonnin, D., et al. (2011). Synthesis of amorphous MgO-rich peridotitic starting material for laser-heated diamond anvil cell experiments—Application to iron partitioning in the mantle. *High Pressure Research*, *31*(1), 199–213. https://doi.org/10.1080/08957959.2011.556631

Badro, J., Brodholt, J. P., Piet, H., Siebert, J., & Ryerson, F. J. (2015). Core formation and core composition from coupled geochemical and geophysical constraints. *Proceedings of the National Academy of Science*, *112*(40), 12,310–12,314. https://doi.org/10.1073/pnas.1505672112

Badro, J., Côté, A. S., & Brodholt, J. P. (2014). A seismologically consistent compositional model of Earth's core. *Proceedings of the National Academy of Science*, *111*(21), 7542–7545. https://doi.org/10.1073/pnas.1316708111

Badro, J., Fiquet, G., Guyo, T. F., Gregoryanz, E., Occelli, F., Antonangeli, D., & d'Astuto, M. (2007). Effect of light elements on the sound velocities in solid iron: Implications for the composition of Earth's core. *Earth and Planetary Science Letters*, *254*, 233–238.

Badro, J., Siebert, J., & Nimmo, F. (2016). An early geodynamo driven by exsolution of mantle components from the Earth's core. *Nature*, *536*(7616), 326–328. https://doi.org/10.1038/nature18594

Barrat, J. A., Zanda, B., Moynier, F., Bollinger, C., Liorzou, C., & Bayon, G. (2012). Geochemistry of CI chondrites: Major and trace elements, and Cu and Zn isotopes. *Geochimica et Cosmochimica Acta*, *83*, 79–92. https://doi.org/10.1016/j.gca.2011.12.011

Benedetti, L. R., & Loubeyre, P. (2004). Temperature gradients, wavelength-dependent emissivity, and accuracy of high and very-high temperatures measured in the laser-heated diamond cell. *High Pressure Research*, *24*(4), 423–445. https://doi.org/10.1080/08957950412331331718

Bischoff, A., Palme, H., Schultz, L., Weber, D., Weber, H. W., & Spettel, B. (1993). Acfer 182 and paired samples, an iron-rich carbonaceous chondrite: Similarities with ALH85085 and relationship to CR chondrites. *Geochimica et Cosmochimica Acta*, *57*(11), 2631–2648. https://doi.org/10.1016/0016-7037(93)90422-S

Blanchard, I., Siebert, J., Borensztajn, S., & Badro, J. (2015). Composition of the core from gallium metal-silicate partitioning experiments. *Earth and Planetary Science Letters*, *427*, 191–201. https://doi.org/10.1016/j.epsl.2015.06.063

Blanchard, I., Siebert, J., Borensztajn, S., & Badro, J. (2017). The solubility of heat-producing elements in Earth's core. *Geochemical Perspectives Letters*, *5*, 1–5.

Bollard, J., Connelly, J. N., Whitehouse, M. J., Pringle, E. A., Bonal, L., Jørgensen, J. K., et al. (2017). Early formation of planetary building blocks inferred from Pb isotopic ages of chondrules. *Science Advances*, *3*(8), e1700407. https://doi.org/10.1126/sciadv.1700407

Bottke, W. F., Walker, R. J., Day, J. M., Nesvorny, D., & Elkins-Tanton, L. (2010). Stochastic late accretion to Earth, the Moon, and Mars. *Science*, *330*(6010), 1527–1530. https://doi.org/10.1126/science.1196874

Brenan, J. M., & Mcdonough, W. F. (2009). Core formation and metal-silicate fractionation of osmium and iridium from gold. *Nature Geoscience*, *2*, 1–4.

Buono, A. S., & Walker, D. (2011). The Fe-rich liquidus in the Fe-FeS system from 1bar to 10GPa. *Geochimica et Cosmochimica Acta*, *75*(8), 2072–2087. https://doi.org/10.1016/j.gca.2011.01.030

Campbell, A. J., & Humayun, M. (2004). Formation of metal in the CH chondrites ALH 85085 and PCA 91467. *Geochimica et Cosmochimica Acta*, *68*(16), 3409–3422. https://doi.org/10.1016/j.gca.2003.11.007

Canup, R. M., Visscher, C., Salmon, J., & Fegley, B. Jr. (2015). Lunar volatile depletion due to incomplete accretion within an impact-generated disk. *Nature Geoscience*, *8*, 918–921. https://doi.org/10.1038/NGEO2574

Chabot, N. L., & Agee, C. B. (2003). Core formation in the Earth and Moon: New experimental constraints from V, Cr, and Mn. *Geochimica et Cosmochimica Acta*, *67*(11), 2077–2091. https://doi.org/10.1016/S0016-7037(02)01272-3

Chabot, N. L., Saslow, S. A., McDonough, W. F., & Jones, J. H. (2009). An investigation of the behaviour of Cu and Cr during iron meteorite crystallization. *Meteoritics and Planetary Science*, *44*(4), 505–519. https://doi.org/10.1111/j.1945-5100.2009.tb00747.x

Chambers, J. E. (2004). Planetary accretion in the inner solar system. *Earth and Planetary Science Letters*, *223*(3-4), 241–252. https://doi.org/10.1016/j.epsl.2004.04.031

Chidester, B. A., Rahman, Z., Righter, K., & Campbell, A. J. (2017). Metal-silicate partitioning of U: Implications for the heat budget of the core and evidence for reduced U in the mantle. *Geochimica et Cosmochimica Acta*, *199*, 1–12. https://doi.org/10.1016/j.gca.2016.11.035

Corgne, A., Keshav, S., Wood, B. J., McDonough, W. F., & Fei, Y. (2008). Metal-silicate partitioning and constraints on core composition and oxygen fugacity during Earth accretion. *Geochimica et Cosmochimica Acta*, *72*(2), 574–589. https://doi.org/10.1016/j.gca.2007.10.006

Cuzzi, J. N., Hogan, R. C., & Shariff, K. (2008). Towards planetessimals: Dense chondrule clumps in the protoplanetary nebula. *The Astrophysical Journal*, *687*(2), 1432–1447. https://doi.org/10.1086/591239

Deguen, R., Landeau, M., & Olson, P. (2014). Turbulent metal-silicate mixing, fragmentation, and equilibration in magma oceans. *Earth and Planetary Science Letters*, *391*, 274–287. https://doi.org/10.1016/j.epsl.2014.02.007

Dreibus, G., & Palme, H. (1996). Cosmochemical constraints on the sulfur content in the Earth's core. *Geochimica et Cosmochimica Acta*, *60*(7), 1125–1130. https://doi.org/10.1016/0016-7037(96)00028-2

Fiquet, G., Auzende, A. L., Siebert, J., Corgne, A., Bureau, H., Ozawa, H., & Garbarino, G. (2010). Melting of peridotite to 140 Gigapascals. *Science*, *329*(5998), 1516–1518. https://doi.org/10.1126/science.1192448

Fischer, R. A., Campbell, A. J., & Ciesla, F. J. (2017). Sensitivities of Earth's core and mantle compositions to accretion and differentiation processes. *Earth and Planetary Science Letters*, *458*, 252–262. https://doi.org/10.1016/j.epsl.2016.10.025

Fischer, R. A., Nakajima, Y., Campbell, A. J., Frost, D. J., Harries, D., Langenhorst, F., & Rubie, D. C. (2015). High pressure metal-silicate partitioning of Ni, Co, V, Cr, Si, and O. *Geochimica et Cosmochimica Acta*, *167*, 177–194. https://doi.org/10.1016/j.gca.2015.06.026

Georg, R. B., Halliday, A. N., Schauble, E. A., & Reynolds, B. C. (2007). Silicon in the Earth's core. *Nature*, *447*(7148), 1102–1106. https://doi.org/10.1038/nature05927

Goldschmidt, V. M. (1922). Über die massenverteilung im erdinneren, verglichen mit der struktur gewisser meteoriten. *Naturwissenschaften*, *10*(42), 918–920. https://doi.org/10.1007/BF01566019

Grossman, J. N., & Wasson, J. T. (1983). The composition of chondrules in unequilibrated chondrites: An evaluation of models for the formation of chondrules and their precursor materials. In E. A. King (Ed.), Chondrules and their origins (pp. 88–121). Houston, TX: Lunar and Planetary Science Institute.

Halliday, A. N. (2013). The origins of volatiles in the terrestrial planets. *Geochimica et Cosmochimica Acta*, *105*, 146–171. https://doi.org/10.1016/j.gca.2012.11.015

Halliday, A. N., & Wood, B. J. (2009). How did Earth accrete? *Science*, *325*(5936), 44–45. https://doi.org/10.1126/science.1172587

Hewins, R. H., & Herzberg, C. T. (1996). Nebular turbulence, chondrule formation, and the composition of the Earth. *Earth and Planetary Science Letters*, *144*(1-2), 1–7. https://doi.org/10.1016/0012-821X(96)00159-8

Hezel, D. C., Harak, M., & Libourel, G. (2018). What we know about elemental bulk chondrule and matrix compositions: Presenting the ChondriteDB database. *Chemie der Erde*, *78*(1), 1–14. https://doi.org/10.1016/j.chemer.2017.05.003

Hin, R. C., Burkhardt, C., Schmidt, M. W., Bourdon, B., & Kleine, T. (2013). Experimental evidence for Mo isotope fractionation between metal and silicate liquids. *Earth and Planetary Science Letters*, *379*, 38–48. https://doi.org/10.1016/j.epsl.2013.08.003

Holzheid, A., & Lodders, K. (2001). Solubility of copper in silicate melts as a function of oxygen and sulfur fugacities, temperature, and silicate composition. *Geochimica et Cosmochimica Acta*, *65*(12), 1933–1951. https://doi.org/10.1016/S0016-7037(01)00545-2

Ivanova, M. A., & Petaev, M. I. (2015). Characteristics and origin of components of the carbonaceous chondrite NWA 470. *Petrology*, *23*(2), 150–167. https://doi.org/10.1134/S0869591115020058

Jacobsen, S. A., & Walsh, K. J. (2015). Earth and terrestrial planet formation. In J. Badro & M. J. Walter (Eds.), *The early Earth: Accretion and differentiation*, *Geophysical Monograph Series* (Vol. 212, pp. 71–82). Hoboken, NJ: John Wiley & Sons. https://doi.org/10.1002/9781118860359.ch3

Johansen, A., Low, M.-M. M., Lacerda, P., & Bizarro, M. (2015). Growth of asteroids, planetary embryos, and Kuiper belt objects by chondrule accretion. *Science*, *1*, e1500109.

Kato, C., & Moynier, F. (2017). Gallium isotopic evidence ofr the fate of moderately volatile elements in planetary bodies and refractory inclusions. *Earth and Planetary Science Letters*, *479*, 330–339. https://doi.org/10.1016/j.epsl.2017.09.028

Laurenz, V., Rubie, D. C., Frost, D. J., & Vogel, A. K. (2016). The importance of sulfur for the behaviour of highly siderophile elements during Earth's differentiation. *Geochimica et Cosmochimica Acta*, *194*, 123–138. https://doi.org/10.1016/j.gca.2016.08.012

Levison, H. F., Kretke, K. A., Walsh, K. J., & Bottke, W. F. (2015). Growing the terrestrial planets from the gradual accumulation of submeter-sized objects. *Proceedings of the National Academy of Sciences*, *112*(46), 14,180–14,185. https://doi.org/10.1073/pnas.1513364112

Li, J., & Agee, C. B. (1996). Geochemistry of mantle-core differentiation at high pressure. *Nature*, *381*(6584), 686–689. https://doi.org/10.1038/381686a0

Libourel, G., & Portail, M. (2018). Chondrules as direct thermochemical sensors of solar protoplanetary disk gas. *Science Advances*, *4*, eaar3321.

Lodders, K. (2003). Solar system abundances and condensation temperatures of the elements. *The Astrophysical Journal*, *591*(2), 1220–1247. https://doi.org/10.1086/375492

Lodders, K., & Fegley, B. Jr. (1998). *The planetary scientist's companion* (pp. 311–317). Oxford: Oxford University Press.

Lord, O. T., Walter, M. J., Dobson, D. P., Armstrong, L., Clark, S. M., & Kleppe, A. (2010). The FeSi phase diagram to 150 GPa. *Journal of Geophysical Research*, *115*, B06209. https://doi.org/10.1029/2009JB006528

Luck, J. M., Othman, B. D., & Albarède, F. (2005). Zn and Cu isotopic variations in chondrites and iron meteorites: Early solar nebula reservoirs and parent-body processes. *Geochimica et Cosmochimica Acta*, *69*(22), 5351–5363. https://doi.org/10.1016/j.gca.2005.06.018

Ma, Z. (2001). Thermodynamic description for concentrated metallic solutions using interaction parameters. *Metallurgical and Materials Transactions B: Process Metallurgy and Materials Processing Science*, *32*(1), 87–103. https://doi.org/10.1007/s11663-001-0011-0

Mahan, B. M., Moynier, F., Siebert, J., Gueguen, B., Agranier, A., Pringle, E. A., et al. (2018). Volatile element evolution of chondrules through time. *Proceedings of the National Academy of Sciences*, *115*(34), 8547–8552. https://doi.org/10.1073/pnas.1807263115

Mahan, B. M., Siebert, J., Blanchard, I., Borensztajn, S., Badro, J., & Moynier, F. (2018). Constraining compositional proxies for Earth's accretion and core formation through high pressure and high temperature Zn and S metal-silicate partitioning. *Geochimica et Cosmochimica Acta*, *235*, 21–40. https://doi.org/10.1016/j.gca.2018.04.032

Mahan, B. M., Siebert, J., Pringle, E. A., & Moynier, F. (2017). Elemental partitioning and isotopic fractionation of Zn between metal and silicate and geochemical estimation of the S content of the Earth's core. *Geochimica et Cosmochimica Acta*, *196*, 252–270.

McDonough, W. F. (2003). Compositional model for the Earth's core. In R. W. Carlson (Ed.), *Treatise on geochemistry* (Vol. 2, pp. 547–568). Oxford: Elsevier-Pergamon. https://doi.org/10.1016/B0-08-043751-6/02015-6

McDonough, W. F., & Sun, S.-S. (1995). The composition of the Earth. *Chemical Geology*, *120*(3-4), 223–253. https://doi.org/10.1016/0009-2541(94)00140-4

Morard, G., Sanloup, C., Fiquet, G., Mezouar, M., Rey, N., Poloni, R., & Beck, P. (2007). Structure of eutectic Fe-FeS melts up to 17 GPa: Implications for planetary cores. *Earth and Planetary Science Letters*, *263*(1-2), 128–139. https://doi.org/10.1016/j.epsl.2007.09.009

Morard, G., Siebert, J., Andrault, D., Guignot, N., Garbarino, G., Guyot, F., & Antonangeli, D. (2013). The Earth's core composition from high pressure density measurements of liquid iron alloys. *Earth and Planetary Science Letters*, *373*, 169–178. https://doi.org/10.1016/j.epsl.2013.04.040

Nimmo, F., O'Brien, D. P., & Kleine, T. (2010). Tungsten isotope evolution during late-stage accretion: Constraints on Earth-Moon equilibration. *Earth and Planetary Science Letters*, *292*(3-4), 363–370. https://doi.org/10.1016/j.epsl.2010.02.003

O'Neill, H. S. C. (1991). The origin of the Moon and the early history of the Earth—A chemical model. Part 1: The Moon. *Geochimica et Cosmochimica Acta*, *55*, 1135–1157.

O'Neill, H. S. C., Canil, D., & Rubie, D. C. (1998). Oxide-metal equilibria to 2500°C and 25 GPa: Implications for core formation and the light component in the Earth's core. *Journal of Geophysical Research*, *13*, 12,239–12,260.

Palme, H., & Jones, A. (2003). Solar system abundances of the elements. In H. D. Holland & K. K. Turekian (Eds.), *Treatise on geochemistry* (Vol. 1, pp. 41–61). Oxford: Elsevier-Pergamon. https://doi.org/10.1016/B0-08-043751-6/01060-4

Palme, H., & O'Neill, H. S. C. (2014). Cosmochemical estimates of mantle composition. In R. W. Carlson (Ed.), *Treatise on geochemistry* (Vol. 2, pp. 1–28). Oxford: Elsevier-Pergamon. https://doi.org/10.1016/B978-0-08-095975-7.00201-1

Piet, H., Badro, J., & Gillet, P. (2017). Geochemical constraints on the size of the Moon-forming giant impact. *Geophysical Research Letters*, *44*, 11,770–11,777. https://doi.org/10.1002/2017GL075225

Pignatale, F. C., Gonzalez, J.-F., Cuello, N., Bourdon, B., & Fitoussi, C. (2017). Size and density sorting of dust grains in SPH simulations of protoplanetary disks. *MNRAS*, *469*(1), 237–254. https://doi.org/10.1093/mnras/stx801

Pignatale, F. C., Liffman, K., Maddison, S. T., & Brook, G. (2016). 2D condensation model for the inner solar nebula: An enstatite-rich environment. *MNRAS*, *457*(2), 1359–1370. https://doi.org/10.1093/mnras/stv3003

Pringle, E. A., & Moynier, F. (2017). Rubidium isotopic composition of the Earth, metorites, and the Moon: Evidence for the origin of volatile loss during planetary accretion. *Earth and Planetary Science Letters*, *473*, 62–70. https://doi.org/10.1016/j.epsl.2017.05.033

Pringle, E. A., Moynier, F., Beck, P., Paniello, R., & Hezel, D. C. (2017). The origin of volatile element depletions in early solar system material: Clues from Zn isotopes in chondrules. *Earth and Planetary Science Letters*, *468*, 62–71. https://doi.org/10.1016/j.epsl.2017.04.002

Righter, K., Drake, M. J., & Scott, E. R. D. (2006). Compositional relationships between meteorites and terrestrial planets. In D. S. Lauretta, & H. Y. McSween, Jr. (Eds.), *Meteorites and the Early Solar System II* (pp. 803–828). Tucson: University of Arizona Press.

Righter, K., Drake, M. J., & Yaxley, G. (1997). Prediction of siderophile element metal-silicate partition coefficients to 20 GPa and 2800°C: The effects of pressure, temperature, oxygen fugacity and silicate and metal melt compositions. *Physics of the Earth and Planetary Interiors*, *100*(1-4), 115–134. https://doi.org/10.1016/S0031-9201(96)03235-9

Righter, K., Pando, K. M., Danielson, L., & Lee, C. T. (2010). Partitioning of Mo, P and other siderophile elements (Cu, Ga, Sn, Ni, Co, Cr, Mn, V, and W) between metal and silicate melts as a function of temperature and silicate melt composition. *Earth and Planetary Science Letters*, *291*(1-4), 1–9. https://doi.org/10.1016/j.epsl.2009.12.018

Rubie, D. C., Jacobson, S. A., Morbidelli, A., O'Brien, D. P., Young, E. D., de Vries, J., et al. (2015). Accretion and differentiation of the terrestrial planets with implications for the compositions of early-formed solar system bodies and accretion of water. *Icarus*, *248*, 89–108. https://doi.org/10.1016/j.icarus.2014.10.015

Rubie, D. C., Laurenz, V., Jacobson, S. A., Morbidelli, A., Palme, H., Vogel, A. K., & Frost, D. J. (2016). Highly siderophile elements were stripped from Earth's mantle by iron sulfide segregation. *Science*, *353*(6304), 1141–1144. https://doi.org/10.1126/science.aaf6919

Rudge, J. F., Kleine, T., & Bourdon, B. (2010). Broad bounds on Earth's accretion and core formation constrained by geochemical models. *Nature Geoscience*, *3*(6), 439–443. https://doi.org/10.1038/ngeo872

Sanloup, C., Drewit, J. W. E., Konôpková, Z., Dalladay-Simpson, P., Morton, D. M., Rai, N., et al. (2013). Structural change in molten basalt at deep mantle conditions. *Nature*, *503*(7474), 104–107. https://doi.org/10.1038/nature12668

Savage, P. S., Moynier, F., Chen, H., Shofner, G., Siebert, J., Badro, J., & Puchtel, I. S. (2015). Copper isotope evidence for large-scale sulphide fractionation during Earth's differentiation. *Geochemical Perspectives Letters*, *1*, 53–64.

Schmitt, W., Palme, H., & Wänke, H. (1989). Experimental determination of metal/silicate partition coefficients for P, Co, Ni, Cu, Ga, Ge, Mo, and W and some implications for the early evolution of Earth. *Geochimica et Cosmochimica Acta*, *53*(1), 173–185. https://doi.org/10.1016/0016-7037(89)90284-6

Schönbächler, M., Carlson, R. W., Horan, M. F., Mock, T. D., & Hauri, E. H. (2010). Heterogeneous accretion and the moderately volatile element budget of Earth. *Science*, *328*(5980), 884–887. https://doi.org/10.1126/science.1186239

Seagle, C. T., Campbell, A. J., Heinz, G. S., & Prakapenka, V. B. (2006). Theraml equation of state of Fe3S and implications for sulfur in Earth's core. *Journal of Geophysical Research*, *111*, B06209. https://doi.org/10.1029/2005JB004091

Shahar, A., Hillgren, V. J., Young, E. D., Fei, Y., Macris, C. A., & Deng, L. (2011). High-temperature Si isotope fractionation between iron metal and silicate. *Geochimica et Cosmochimica Acta*, *75*(23), 7688–7697. https://doi.org/10.1016/j.gca.2011.09.038

Siebert, J., Badro, J., Antonangeli, D., & Ryerson, F. J. (2012). Metal-silicate partitioning of Ni and Co in a deep magma ocean. *Earth and Planetary Science Letters*, *321-322*, 189–197. https://doi.org/10.1016/j.epsl.2012.01.013

Siebert, J., Badro, J., Antonangeli, D., & Ryerson, F. J. (2013). Terrestrial accretion under oxidizing conditions. *Science*, *339*(6124), 1194–1197. https://doi.org/10.1126/science.1227923

Siebert, J., Corgne, A., & Ryerson, F. J. (2011). Systematics of metal-silicate partitioning for many siderophile elements applied to Earth's core formation. *Geochimica et Cosmochimica Acta*, *75*(6), 1451–1489. https://doi.org/10.1016/j.gca.2010.12.013

Siebert, J., & Shahar, A. (2015). An experimental geochemistry perspective on Earth's core formation. The Early Earth: accretion and differentiation. *Geophysical Monograph*, *212*(1), 103–121.

Siebert, J., Sossi, P. A., Blanchard, I., Mahan, B., Badro, J., & Moynier, F. (2018). Chondritic Mn/Na ratio and limited post-nebular volatile loss of the Earth. *Earth and Planetary Science Letters*, *485*, 130–139. https://doi.org/10.1016/j.epsl.2017.12.042

Sossi, P. A., Nebel, O., O'Neill, H. S. C., & Moynier, F. (2018). Zinc isotope composition of the Earth and its behaviour during planetary accretion. *Chemical Geology*, *477*, 73–84. https://doi.org/10.1016/j.chemgeo.2017.12.006

Stewart, S.T., Lock, S.J., Petaev, M.I., Jacobsen, S.B., Sarid, G., Leinhardt, M., et al. (2016).Mercury impact origin hypothesis survives the volatile crisis: Implications for terrestrial planet formation. *47th Lunar and Planetary Science Conference* (Abstract 2954).

Suer, T.-A., Siebert, J., Remusat, L., Menguy, N., & Fiquet, G. (2017). A sulfur-poor terrestrial core inferred from metal-silicate partitioning experiments. *Earth and Planetary Science Letters*, *469*, 84–97.

The Japan Society for the Promotion of Science and The Nineteenth Committee on Steelmaking (1988). Part 2: Recommended values of activity and activity coefficients, and interaction parameters of elements in iron alloys. In *Steelmaking Data Sourcebook* (pp. 273–297). New York: Gordon and Breach Science Publishers.

Tonks, W. B., & Melosh, H. J. A. Y. (1993). Magma ocean formation due to giant impacts. *Journal of Geophysical Research*, *98*(E3), 5319–5333. https://doi.org/10.1029/92JE02726

Vogel, A. K. (2015). Siderophile element partitioning at high pressure and temperatures—Implications for core formation processes, (PhD thesis). Universität Bayreuth, Germany.

Vollstaedt, H., Mezger, K., & Leya, I. (2016). The isotopic composition of selenium in chondrites constrains the depletion mechanism of volatile elements in solar system materials. *Earth and Planetary Science Letters*, *450*, 372–380. https://doi.org/10.1016/j.epsl.2016.06.052

Wade, J., & Wood, B. J. (2005). Core formation and the oxidation state of the Earth. *Earth and Planetary Science Letters*, *236*(1-2), 78–95. https://doi.org/10.1016/j.epsl.2005.05.017

Wade, J., & Wood, B. J. (2016). The oxidation state and mass of the Moon-forming impactor. *Earth and Planetary Science Letters*, *442*, 186–193. https://doi.org/10.1016/j.epsl.2016.02.053

Wade, J., Wood, B. J., & Tuff, J. (2012). Metal-silicate partitioning of Mo and W at high pressures and temperatures: Evidence for late accretion of sulphur to the earth. *Geochimica et Cosmochimica Acta*, *85*, 58–74. https://doi.org/10.1016/j.gca.2012.01.010

Wang, K., & Jacobsen, S. (2016). An estimate of the bulk silicate earth potassium isotopic composition based on MC-ICPMS measurements of basalts. *Geochimica et Cosmochimica Acta*, *178*, 223–232. https://doi.org/10.1016/j.gca.2015.12.039

Wang, Z., Laurenz, V., Petitgirard, S., & Becker, H. (2016). Earth's moderately volatile element composition may not be chondritic: Evidence from in, Cd and Zn. *Earth and Planetary Science Letters*, *435*, 136–146. https://doi.org/10.1016/j.epsl.2015.12.012

Weisberg, M. K., McCoy, T. J., & Krot, A. N. (2006). Systematics and evaluation of meteorite classification. In D. S. Lauretta & H. Y. McSween, Jr. (Eds.), *Meteorites and the early solar system II* (pp. 19–52). Tucson: University of Arizona Press.

Wetherill, G. W. (1989). The formation of the solar system: Consensus, alternatives, and missing factors. In H. A. Weaver & L. Danly (Eds.), *The formation and evolution of planetary systems* (pp. 1–30). Cambridge, New York: Cambridge University Press.

Wohlers, A., & Wood, B. (2015). A Mercury-like component of early Earth yields uranium in the core and high mantle 142ND. *Nature*, *520*(7547), 337–340. https://doi.org/10.1038/nature14350

Wombächer, F., Rehkämper, M., Mezger, K., Bischoff, A., & Münker, C. (2008). Cadmium stable isotope cosmochemistry. *Geochimica et Cosmochimica Acta*, *72*, 646–667.

Wood, B. J., Kiseeva, E. S., & Mirolo, F. J. (2014). Accretion and core formation: The effects of sulfur on metal-silicate partition coefficients. *Geochimica et Cosmochimica Acta*, *145*, 248–267. https://doi.org/10.1016/j.gca.2014.09.002

Wood, B. J., Walter, M. J., & Wade, J. (2006). Accretion of the Earth and segregation of its core. *Nature*, *441*(7095), 825–833. https://doi.org/10.1038/nature04763

Zhang, Y., Sekine, T., He, H., Yu, Y., Liu, F., & Zhang, M. (2016). Experimental constraints on light elements in the Earth's outer core. *Scientific Reports*, *6*, e22473.